HOKKAIDO UNIVERSITY

Title	A liquid metal catalyst for the conversion of ethanol into graphitic carbon layers under an ultrasonic cavitation field
Author(s)	Kawasaki, Hideya; Otsuki, Tomoko; Sugino, Fumiya et al.
Citation	Chemical communications, 58(56), 7741-7744 https://doi.org/10.1039/d2cc02510h
Issue Date	2022-07-18
Doc URL	https://hdl.handle.net/2115/90169
Type	journal article
File Information	manuscript R1.pdf

ChemComm

Liquid metal catalyst for the conversion of ethanol into graphitic carbon layers under ultrasonic cavitation field

Hideya Kawasaki,[*a] Tomoko Otsuki,[a] Fumiya Sugino,[b] Ken Yamamoto,[b] Tomoharu Tokunaga,[c] Rintaro Tokura,[d] Tetsu Yonezawa[*d]

Eutectic Gallium Indium (EGaIn) has drawn considerable research interest in potential liquid catalysis. Herein, we report that EGaIn liquid metal acts as a catalyst for the growth of graphitic carbon layer from ethanol under ultrasonication. High-speed imaging demonstrated the formation of ultrasonic cavitation bubbles at the liquid metal/ethanol interface, which facilitated the pyrolysis of ethanol into graphitic carbon on the liquid metal surface.

Liquid metals are alloys with low melting points and exist as a liquid at temperatures lower than 200 °C. Among them, Ga-based liquid metals, such as an eutectic alloy of Ga and In (EGaIn; 75.5% Ga and 24.5% In by weight), have a relative low melting point and are liquid at near room temperature (melting points of Ga and EGaIn are 29.8 and 15 °C, respectively).[1] In contrast to mercury, which is the most common liquid metal, Ga-based liquid metals have significantly low vapor pressure, and thus, they are safer. Ga-based liquid metals have drawn considerable research interest because of their unique properties such as high electrical and thermal conductivity, low toxicity, low viscosity, and high metal solubility.[2] In addition to the solid-based micro-and nano-sized metal particles, micro- and nano-sized liquid metal particles (LMP) have emerged as a new category of particle systems.[3] Owing to the unique properties of LMP, such as high surface area, high surface functionality, broad temperature range of the liquid state, and stimuli-responsive coalescence, LMP have immense application potential in electronics, catalysis, energy storage/conversion, and biomedical fields.[3] To date, majority of the investigations on Ga-based liquid metals and their particles have focused on their applications in electronics, such as flexible/stretchable electronic devices,[4,5] actuators,[6] sensors,[7] robotics,[8] and soft metal components, for human-machine interfaces.[9,10] More recently, there has been a growing interest in interfacial engineering of liquid metals for potential active catalysis[11-13] such as fabrication of nanostructured 2D materials including graphene via chemical vapor deposition(CVD),[14-17] metal oxide nanosheet formation,[18] hydrogen production via water splitting,[19] dehydrogenations of hydrocarbon,[20] sonocatalytic degradations of organic dyes,[21] and photocatalysis.[22]

Ultrasonication is a common method for preparing LMP.[3] An intense ultrasonic irradiation produces numerous smaller liquid droplets (i.e., LMP) owing to the sonication-induced mechanical agitation and acoustic cavitation. The acoustic cavitation effect is a unique feature of ultrasonication and involves ultrasound-induced nucleation, growth, and collapse of microbubbles.[23,24] The cavitation-induced hotspots are regions of high temperature (~5000 K) and high pressure (~2000 atm) and are formed in the liquid at immediately after the bubble collapse, leading to chemical reactions such as pyrolysis of solvent vapors into free radicals (e.g., conversion to hydroxyl radicals via pyrolysis of water).[23,24] Moreover, the bubble implosion creates shock waves within the liquid, promoting the mixing and fragmentation of its droplets (i.e., a physical effect).[23,24] These ultrasonic-induced physical and chemical events are highly favored at the liquid metal/solvent interfaces of LMP because of the increased specific surface area resulting from multiple cycles of droplet splitting under ultrasonication. Thus far, researchers have utilized the physical effects of ultrasonic treatment for the size refinement and dispersion of LMP. However, little attention has been given to the chemical effects of ultrasonic treatment at the liquid metal/solvent interface of LMP. Previous research has demonstrated thermal catalysis of

ᵃDepartment of Chemistry and Materials Engineering, Faculty of Chemistry, Materials and Bioengineering, Kansai University, Suita-shi, Osaka 564-8680, Japan.
E-mail: hkawa@kansai-u.ac.jp (H.K)
ᵇDepartment of Pure and Applied Physics, The Faculty of Engineering Science, Kansai University, Suita-shi, Osaka 564-8680, Japan.
ᶜDepartment Materials Science and Engineering, Faculty of Engineering, Nagoya University, Furo-Cho, Nagoya 464-8603, Japan.
ᵈDivision of Materials Science and Engineering, Faculty of Engineering, Hokkaido University, Sapporo 060-8628, Japan.
E-mail: tetsu@eng.hokudai.ac.jp (T.Y)
† Electronic Supplementary Information (ESI) available: EGaIn particle preparation and their characterization, High-speed imaging, TEM and STEM images of LMPs (EtOH), EELS and XPS spectra of LMPs (EtOH) and LMPs (PrOH), UV-Vis spectra of the supernatant solution obtained from LMPs (PrOH), SEM images of LMPs (EtOH) and LMPs (PrOH), Photographs of LMPs (EtOH) and LMPs(PrOH) dispersion, and SEM images of their sediments. See DOI: 10.1039/x0xx00000x

liquid metals at high temperatures of more than 500 °C, such as gaseous methane to hydrogen,[25] and gaseous CO_2 to solid carbon.[26] Thus,we expected that ultrasonically-induced cavitations with high temperatures (i.e., hotspots) give rise to the thermal catalytic activity of LMP.

Here, we first demonstrate EGaIn-based LMP catalyst for the conversion of ethanol into graphitic carbon layers via the ultrasonic cavitation-induced hotspots. Strong ultrasonic irradiation was applied to a mixture of ethanol and EGaIn in an ice bath to prevent the ethanol evaporation, producing a colloidal dispersion of LMP in ethanol, denoted as LMP(EtOH) hereafter. The transmission electron microscopy(TEM) images of LMP (EtOH)(Figs.1a and 1b) confirmed the presence of carbonaceous materials, along with sheet-like fragments, on the surface of LMP(EtOH) (ESI Fig. S1). The scanning electron microscopy/energy dispersive spectroscopy(SEM-EDS) analysis of the isolated carbonaceous materials revealed that the solid product consists of carbon and oxygen, with trace quantities of Ga and In (Fig.S2). Lin et al. also reported the presence of surface carbon layers of LMP(EtOH).[28] However, the formation mechanism of the surface carbon layer has not been clarified yet. In addition, it has also been pointed out that there is a possibility of the adventitious amorphous carbon layer usually detected on sample surfaces in air.[29]

To investigate the chemical state of the C atoms of the LMP(EtOH) surface, we performed spatially resolved transmission electron microscopy-electron energy loss spectroscopy (TEM-EELS) of the LMP(EtOH) surface. For comparison, LMP were prepared in 1-propanol instead of ethanol, and this system will be denoted as LMP(PrOH) hereafter. The sharp EELS peaks at ~292 eV at the carbon K-edge are attributable to the 1s–σ* transition from the sp³-hybridized C atoms (Fig. 1c and Fig. S3a),[30] confirming the presence of the carbon layer on the LMP(EtOH) surface. More importantly, the small peak at 282 eV corresponded to the 1s–π*transitions from sp² graphitic carbon, confirming the formation of a graphitic carbon layer.[30] The weak peak from the 1s–π*transition suggests the thin layer and a small fraction of the graphitic component in the surface carbon layer of LMP(EtOH). In contrast, TEM-EELS analysis of the LMP(PrOH) surface showed no peak corresponding to an sp² graphitic structure (Fig. 1d and Fig. S3b). Thus, the graphitic carbon layer was formed only on the LMP(EtOH) surface and not on the LMP (PrOH) surface.
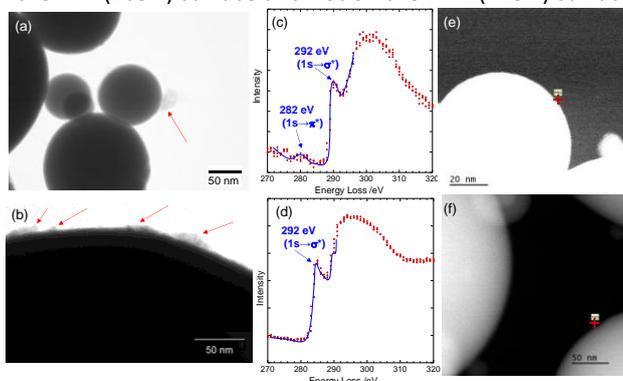

Fig. 1. (a) and (b) TEM images of LMP(EtOH). Red arrows indicate the carbonaceous materials. EELS spectra of carbon K-edge (1s) for (c) LMP(EtOH) and

(d)LMP(PrOH) recorded at the surface of the LMP(indicated with a red cross in the STEM images for (e) LMP(EtOH) and (f) LMP(PrOH)).

X-ray photoelectron spectroscopy (XPS) of LMP(EtOH) and LMP(PrOH) was recorded to investigate the characteristic differences in forming surface carbon. The wide-scan XPS spectra revealed the presence of Ga, In, O, and C for both LMP (EtOH) and LMP(PrOH), as shown in Fig. S4. The narrow scan XPS spectrum of LMP(EtOH) shows C1s peak with an asymmetric tail towards lower binding energy, corresponding to sp² carbon (area = 22.1%) at 284.4 eV, C-O bonds (area = 12.5%) at 286.3 eV, C=O bonds at 287.7 eV (area = 2.1 %), and O=C-O bonds at 289.2 eV (area =1.9%) in the C 1s region, besides sp³ amorphous carbon (area = 61.4%) at 285. 0 eV (Fig. 2a).[31] In contrast, no peaks corresponding to sp² carbon were observed in the C 1s region for LMP(PrOH), and the main peak corresponded to sp³ amorphous carbon (area % = 92.9 %) (Fig. 2b). Thus, the XPS spectrum of LMPs(EtOH) indicated the presence of oxidized graphitic carbonaceous materials (probably, graphene oxide). Notably, a thin layer of carbonaceous material is often found on the surface of most air-exposed samples, and this layer is generally known as adventitious carbon. Adventitious carbon is sp³ amorphous carbon and does not appear to be graphitic in nature.[32] Thus, we concluded that the sp² carbon on the LMP (EtOH) was not adventitious carbon.

Addition of HCl resulted in the coalescence of LMP(EtOH) owing to the destruction of the surface oxide layers. The resultant sample was centrifuged, and the supernatant, which did not contain LMP, was collected. The UV-Vis spectra of the supernatant showed an absorption peak at ~250 nm due to the n-π* transition of the C=O bonds, which are characteristic of graphene oxide (Fig. 2c).[33] Such peaks corresponding to n-π* transition were not observed for ethanol after ultrasonication for 2 h (Fig. 2c) or for LMP(PrOH) (Fig. S5).
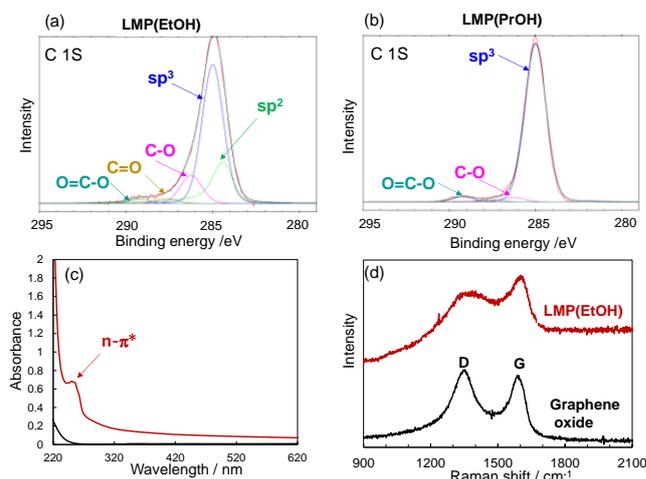

Fig. 2. XPS spectra of the C 1s region of (a)LMP(EtOH) and (b) LMP(PrOH). (c) UV-Vis spectra of the supernatant obtained from the LMP(EtOH) dispersion in ethanol after HCl addition and subsequent centrifugation (solid red line) and that of the ethanol solution obtained under sonication conditions identical to those for LMP(EtOH) formation (solid black line). (d) Raman spectra of LMP(EtOH) and commercially obtained graphene oxide.

To further examine the order level within the produced graphitic carbonaceous material on LMP(EtOH), we performed

Raman spectroscopy of LMP(EtOH). The Raman spectrum showed D and G bands at 1360 and 1600 cm^{-1}, respectively, similar to the case of graphene oxide (Fig. 2d).[34] The G peak originates from the stretching vibrations of the carbon bonds in the rings of the graphitic layers. The G band of LMP(EtOH) was shifted to a higher wavelength compared to that of graphene oxide, suggesting the multilayered structure of the sp^2-hybridized graphene layers.[34] The D band is attributed to defects in the periodic lattice of graphene, and the broadening of the D band occurs owing to higher disorder or more defects in the LMP(EtOH).[34] The relative intensity ratio of the D and G bands (I_D/I_G) was 0.84 for LMP(EtOH), which is smaller than that of graphene oxide (I_D/I_G = 0.93). This indicated a higher density of defects in the sp^2 hybridized graphene layers for LMP(EtOH) compared to that in graphene oxide.

All the above analyses of the carbonaceous material indicate that the oxidized graphitic carbon layers are formed at the LMP/ethanol interface under ultrasonication. It might be interesting to know the reason for the formation of graphitic carbon in the LMP(EtOH) prepared by ultrasonication. Because graphitic carbon is formed only at high temperatures,[35] the ultrasonication-induced cavitation, which too generates a high-temperature environment in ethanol, is likely to induce the pyrolysis of ethanol vapor into carbon precursors for graphene growth on the LMP catalytic surface.

Based on the above speculation, we prepared an experimental setup for the in situ observation of cavitation bubble formation at the EGaIn liquid metal/ethanol interface under ultrasonication using high-speed imaging.[36] The images, captured using a high-speed camera with a time interval of 5 μs in each frame, demonstrated that the cavitation bubbles are preferentially generated at the liquid metal and ethanol interface under ultrasonication (Fig. 3). Video S1 in the supplementary information shows the oscillating bubbles (also shown using white arrows in image I of Fig. 3). In contrast, the black clouds (shown in white circles in images II, III, and IV of Fig. 3) are not found to oscillate (in the Video) and are probably the liquid metal droplets. The cavitation bubble grows up to a specific size and then collapses onto the surface of the LMP. After the implosion of the cavitation bubble at the liquid metal/ethanol interface, shock waves induce the fragmentation of liquid metals into tiny droplets. The violent collapse of the bubbles at the interface generates a highly localized high temperature and pressure environment, causing the pyrolysis of ethanol to form graphitic carbon. Reese et al. demonstrated that ultrasonication causes catalytic decomposition of ethanol into ethylene on the silver catalytic surface.[37] Previous study reported that ethylene adsorption on metal surfaces at high temperatures leads to forming a graphene layer.[38] Thus, it is reasonable to suggest that high-energy ultrasonic cavitation hot spots cause catalytic decomposition of ethanol into ethylene at EGaIn liquid metal/ethanol interface. The ethylene adsorption on the liquid metal surface activates the C−H bond, forming a graphene layer.
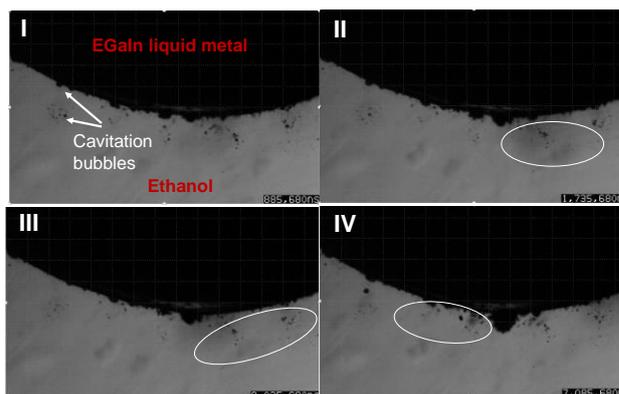

Fig. 3. Snapshots of the dynamic behavior of cavitation bubbles and the EGaIn liquid metal–ethanol interface during ultrasonication: Image I at 885,680 ns, Image II at 1,735,680 ns, Image III at 2,035,680 ns, and Image IV at 7,085,680 ns. The video images were approximately 4.24 mm in width and 2.65 mm in height. The white circles and ellipses indicate the fragmentation of liquid metals into tiny droplets.

The schematic of the proposed liquid metal-catalyzed ethanol conversion to oxidized graphitic carbon layers under an ultrasonic cavitation field is presented in Fig. 4. (I)Cavitation bubbles form on the surface of LMP, and ethanol evaporates into the cavitation bubble during bubble expansion. (II)Upon implosion of the cavitation bubble at the EGaIn–ethanol interface, the ultrasonic cavitation-induced pyrolysis of ethanol into carbonaceous precursors (e.g. ethylene) occurs at the interface as well as the fragmentation of EGaIn. (III)The generated carbon species deposits onto the surface of the EGaIn. (IV) The graphitic carbonaceous materials grow on the catalytic surface of EGaIn liquid metal. The formation of graphitic carbon materials, including graphene, is favored when C2 precursors are the dominant gas-phase species at high temperatures for the growth of aromatic rings.[35,39,40] This explains why the graphitic layer is not formed in the case of C3 species, 1-propanol. Further studies are needed to clarify the catalytic mechanism of liquid metal surfaces under the ultrasonic cavitation field, such as the surface catalyzed chemical pathways and the intermediates.
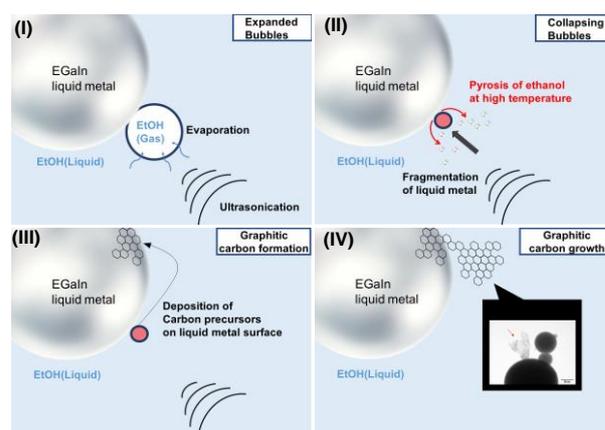

Fig. 4. Proposed formation mechanism of graphitic carbon materials from ethanol at the EGaIn–ethanol interface under ultrasonication.(I)expanded bubbles, (II) collapsing bubbles, (III) carbonaceous precursor formaion, and (IV) graphitic carbon growth.

The graphitic carbon coating of LMP(EtOH) can contribute to the high colloidal stability of LMP(EtOH) against coalescence compared to LMP(PrOH), which does not have a graphitic carbon coating. SEM images of LMP showed broad and similar size distribution (300−800 nm) of LMP(EtOH) and LMP(PrOH) just after sample preparation (Fig. S6). However, high dispersion stability of the LMP was observed only in ethanol. LMP produced in ethanol remained suspended for up to several weeks (Fig. S7a)[28], while sediments of LMP were formed at the bottom of the vial within a few days in 1-propanol (Fig. S7b). The SEM images of the LMP(PrOH) sediments showed large particles, which were formed through coalescence and subsequent growth of these particles in LMP(PrOH) (Fig. S7d). The coalescence was lesser in LMP(EtOH), as shown in Fig. S7c. The stabilizing outer shells of LMP(EtOH) prevent the liquid droplets from coalescing, contributing to the high dispersion stability of LMP(EtOH).

In summary, we have demonstrated the catalytic conversion of ethanol to oxidized graphitic carbon layers under an ultrasonic cavitation field on the surface of EGaIn liquid metal. High-speed imaging revealed that the cavitation bubbles are preferentially generated at the liquid metal–ethanol interface under ultrasonication. The bubbles collapse at the interface violently, generating high pressures and high temperatures that induce the pyrolysis of ethanol vapor. It is proposed that the pyrolysis of ethanol occurs inside the ultrasonic cavitation bubbles, followed by the growth of graphitic carbon layers on the LMP catalytic surface. Previous studies demonstrated that liquid metal could work as thermal conversion catalysis in high-temperature, such as CH_4[25]and CO_2.[26] In contrast, our approach allows catalytic ethanol conversion at low temperatures with the help of ultrasonic high-energy cavitation field. The results presented here offer new insights that the ultrasonic high-energy hot spots create a chemical reaction field at the liquid metal/solution interface for promoting thermally metal-catalyzed reactions. The ultrasonically-activated EGaIn liquid metals would also encourage further research on thermal catalytic conversions such as CO_2[41] and CH_4.[42]

Conflicts of interest
There are no conflicts to declare.

Authorship contributions
H. Kawasaki: the *conceptualization of this study and approval of the final draft,* T. Otsuki: *synthesis of LMP,* F. Sugino: *collection of high-speed imaging,* K. Yamamoto: *design on ultrasonic instruments and interpretation of high-speed imaging,* T. Tokunaga: *data analysis of TEM-EELS, collection, analysis, and interpretation of TEM and TEM-EELS measurement data*, R. Tokura: *data analysis and interpretation of TEM-EELS.* T. Yonezawa: the *design on the characterization of LMP and final draft approval.*

Notes and references
1. W. M. Haynes, CRC Handbook of Chemistry and Physics, 95th ed., CRC Press, Boca Raton, FL 2014.
2. (*a*)T. Daeneke, K. Khoshmanesh, N. Mahmood, I. A. de Castro, D. Esrafilzadeh, S. J. Barrow, M. D. Dickey and K. Kalantar-zadeh, *Chem. Soc. Rev.*, 2018, **47**, 4073; (*b*) F.-M. Allioux, M. B. Ghasemian, W. Xie, A. P. O'Mullane, T. Daeneke, M. D. Dickey and K. Kalantar-Zadeh, *Nanoscale Horiz.*, 2022, **7**, 141.
3. (*a*) C. Chiew, M. J. Morrisa and M. H. Malakooti, *Mater. Adv.*, 2021, **2**, 7799; (b) Y. Liu, W. Zhang and H. Wang, *Mater. Horiz.*, 2021, **8**, 56; (c) S.-Y. Tang and R. Qiao, *Acc. Mater. Res.,* 2021, **2**, 966.
4. J.-E. Park, H.S. Kang, J. Baek, T. H. Park, S. Oh, H. Lee, M. Koo and C. Park, *ACS Nano*, 2019, **13**, 9122.
5. N. Ochirkhuyag, R. Matsuda, Z. Song, F. Nakamura, T. Endo and H. Ota, *Nanoscale*, 2021, **13**, 2113.
6. X. Li, M. Li, J. Xu, J. You, Z. Yang and C. Li, *Nat Commun.*, 2019, **10**, 3514.
7. M. Baharfar and K. Kalantar-Zadeh, *ACS Sens.*, 2022, **7**, 386.
8. Z. Li, J. Xu, Z. Wu, B. Guo and Q. He, *Acc. Mater. Res.,* 2022, **3**, 122.
9. R. Tutika, A. B. M. T. Haque and M. D. Bartlett, *Commun. Mater.*, 2021, **2**, 64.
10. X. Ma, M. Zhang, J. Zhang, S. Wang, S. Cao, Y. Li, G. Hu and D. Kong, *ACS Materials Lett.,* 2022, **4**, 634.
11. S.-T. Liang, H.-Z. Wang and J. Liu, *Chem. Eur. J.,* 2018, **24**, 17616.
12. K. Zuraiqi, A. Zavabeti, F.-M. Allioux , J. Tang, C. K. Nguyen, P. Tafazolymotie, M.Mayyas, A. V. Ramarao, M. Spencer, K. Shah, C. F. McConville, K. Kalantar-Zadeh, K. Chiang and T. Daeneke, *Joule,* 2020, **4**, 2290.
13. J.-H. Fu, T.-Y. Liu, Y. Cui, and J. Liu, *Adv. Mater. Interfaces,* 2021, **8**, 2001936.
14. G. Ding, Y. Zhu, S. Wang, Q. Gong, L. Sun, T. Wu, X. Xie, and M. Jiang, *Carbon,* 2013, **53**, 321.
15. M. Zeng, L. Tan, J. Wang, L. Chen, M. H. Rümmeli and L. Fu, *Chem. Mater.,* 2014, **26**, 12, 3637.
16. M. Zeng and L. Fu, *Acc. Chem. Res.,* 2018, **51**, 2839.
17. C. Tsakonas, M. Dimitropoulos, A. C. Manikas and C. Galiotis, *Nanoscale*, 2021, **13**, 3346.
18. A. Goff, P. Aukarasereenont, C. K. Nguyen, R. Grant, N. Syed, A. Zavabeti, A. Elbourne and T. Daeneke, *Dalton Trans.,* 2021, **50**, 7513.
19. J. Lu, W. Yu, S. Tan, L. Wang, X. Yang and Jing Liu, *RSC Adv.,* 2017, **7**, 30839.
20. N. Taccardi, M. Grabau, J. Debuschewitz, M. Distaso, M. Brandl, R. Hock, F. Maier, C. Papp, J. Erhard, C. Neiss, W. Peukert, A. Görling, H.-P. Steinrück and P. Wasserscheid, *Nature Chem.,* 2017, **9**, 862.
21. F. Hoshyargar, H. Khan, K. Kalantar-zadeh and A. P. O'Mullane, *Chem. Commun.*, 2015, **51**, 14026.
22. W. Zhang, J. Z. Ou, S.-Y. Tang, V. Sivan, D. D. Yao, K. Latham, K. Khoshmanesh, A. Mitchell, A. P. O'Mullane and K. Kalantar-zadeh, *Adv. Funct. Mater.,* 2014, **24**, 3799.
23. L. H. Thompson and L. K. Doraiswamy, *Ind. Eng. Chem. Res.,* 1999, **38**, 1215.
24. H. Xu, B. W. Zeiger and K. S. Suslick, *Chem. Soc. Rev.,* 2013, **42**, 2555.
25. D. C. Upham, V. Agarwal, A. Khechfe, Z. R. Snodgrass, M. J. Gordon, H. Metiu and E. W. McFarland, *Science,* 2017, **358**, 917.
26. K. Zuraiqi, A. Zavabeti, J. Clarke-Hannaford, B. J. Murdoch, K. Shah, M. J. S. Spencer, C. F. McConville, T. Daeneke and K. Chiang, *Energy Environ. Sci.,* 2022, **15**, 595.
27. D. R. G. Mitchell, *Micron,* 2015, **73**, 36.
28. Y. Lin, C. Cooper, M. Wang, J. J. Adams, J. Genzer and M. D. Dickey, *Small,* 2015, **11**, 6397.
29. M. A. Creighton, M. C. Yuen, M. A. Susner, Z. Farrell, B. Maruyama and C. E. Tabor, *Langmuir,* 2020, **36**, 12933.
30. K. Suenag and M. Koshino, *Nature,* 2010, **468**, 1088.
31. M. A. Creighton, M. C. Yuen, N. J. Morris and C. E. Tabor, *Nanoscale,* 2020,**12**, 23995.
32. G. Greczynsk and L. Hultman, *ChemPhysChem,* 2017, **18**, 1507.
33. Q. Lai, S. Zhu, X. Luo, M. Zou and S. Huang, *AIP Adv.,* 2012, **2**, 032146.
34. A. Kaniyoor and S. Ramaprabhu, *AIP Adv.,* 2012, **2**, 032183.
35. P. Fortugno, S. Musikhin, X. Shi, H. Wang, H. Wiggers and C. Schulz, *Carbon,* 2022, **186**, 560.
36. T. Yamamoto, R. Matsutaka and S. V. Komarov, *Ultrason. Sonochem.,* 2021, **71**, 105387.
37. S. J. Reese, D. H. Hurley, and H. W. Rollins, *Ultrason. Sonochem.,*2006, **13**, 283.
38. B. Wang, M. König, C. J. Bromley, B. Yoon, M.-J. Treanor, J. G. Torres, M. Caffio, F. Grillo, H. Früchtl, N. V. Richardson, F. Esch, U. Heiz, U. Landman and R. Schaub, *J. Phys. Chem. C,* 2017, **121**, 9413.
39. C. Melero, R. Rincón, J. Muñoz, G. Zhang, S. Sun, A. Perez, O. Royuela, C. González Gago and M. D. Calzada, *Plasma Phys. Control. Fusion,* 2018, **60**, 014009.
40. J.-J. Koo and Z. H. Kim, *J. Phys. Chem. Lett.,* 2022, **13**, 3740.
41. J. Tang, J. Tang, M. Mayyas, M.B. Ghasemian, J. Sun, M. A. Rahim, J. Yang, J. Han, D. J. Lawes, R. Jalili, et al., *Adv.Mater.,* 2022, **34**, 2105789.
42. J. Tang, P. V. Kumar, J. A. Scott, J. Tang, M. B. Ghasemian, M. Mousavi, J. Han, D. Esrafilzadeh, K. Khoshmanesh, T. Daeneke et al., *ACS Nano,* 2022, https://doi.org/10.1021/acsnano.2c02326